Hinting a dark matter nature of Sgr A∗ via the S-stars

E. A. Becerra-Vergara,[1,2,3]★ C. R. Argüelles,[1,2,4] A. Krut,[1,2] J. A. Rueda [ID][1,2,5,6]★ and R. Ruffini[1,2,5,6]★

[1]*ICRANet, Piazza della Repubblica 10, I-65122 Pescara, Italy*
[2]*ICRA, Dip. di Fisica, Sapienza Università di Roma, P.le Aldo Moro 5, I-00185 Rome, Italy*
[3]*GIRG, Escuela de Física, Universidad Industrial de Santander, 680002 Bucaramanga, Colombia*
[4]*Fac. de Ciencias Astron. y Geofísicas, Universidad Nacional de La Plata, Paseo del Bosque, B1900FWA La Plata, Argentina*
[5]*ICRANet-Ferrara, Dip. di Fisica e Scienze della Terra, Università degli Studi di Ferrara, Via Saragat 1, I-44122 Ferrara, Italy*
[6]*INAF, Istituto di Astrofisica e Planetologia Spaziali, Via Fosso del Cavaliere 100, I-00133 Rome, Italy*

ABSTRACT

The motion data of the S-stars around the Galactic Centre gathered in the last 28 yr imply that Sgr A∗ hosts a supermassive compact object of about $4 \times 10^6\,M_\odot$, a result awarded with the Nobel Prize in Physics 2020. A non-rotating black hole (BH) nature of Sgr A∗ has been uncritically adopted since the S-star orbits agree with Schwarzschild geometry geodesics. The orbit of S2 has served as a test of general relativity predictions such as the gravitational redshift and the relativistic precession. The central BH model is, however, challenged by the G2 post-peripassage motion and by the lack of observations on event-horizon-scale distances robustly pointing to its univocal presence. We have recently shown that the S2 and G2 astrometry data are better fitted by geodesics in the spacetime of a self-gravitating dark matter *core–halo* distribution of 56 keV-fermions, '*darkinos*', which also explains the outer halo Galactic rotation curves. This letter confirms and extends this conclusion using the astrometry data of the 17 best-resolved S-stars, thereby strengthening the alternative nature of Sgr A∗ as a dense core of darkinos.

Key words: Elementary particles – Dark matter.

1 INTRODUCTION

The gravitational potential in the Galactic centre (GC) is dominated by a supermassive compact object, Sagittarius A∗ (Sgr A∗), long thought to be a massive black hole (BH) of $\approx 4 \times 10^6\,M_\odot$ (Ghez et al. 2005, 2008; Genzel, Eisenhauer & Gillessen 2010; Gravity Collaboration 2018b). From the observational viewpoint, this inference on the nature of Sgr A∗ mainly comes from the nearly Keplerian orbits of tens of stars belonging to the S-star cluster (Gillessen et al. 2009a, 2017), whose motions are well described by geodesics in the Schwarzschild spacetime geometry. The most important S-cluster member is S2 which, with an orbital period of about 16 yr and a pericentre of about 1500 Schwarzschild radii, has the most compact orbit around Sgr A∗. The S2 orbit data have allowed to test general relativity predictions such as the relativistic redshift (see e.g. Gravity Collaboration 2018a; Do et al. 2019) and precession (see e.g. Parsa et al. 2017; Gravity Collaboration 2020). However, not every news is good for the BH model; it is challenged by the G2 motion which cannot be explained by any geodesics in the BH geometry (Plewa et al. 2017; Gillessen et al. 2019), as well as by very scarce data at event-horizon-scale distances from Sgr A∗, robustly pointing to a univocal central BH presence (see e.g. Yuan & Narayan 2014; Bouffard et al. 2019).

In view of the above, we have dived into the possibility of an alternative nature for Sgr A∗ based on the fermionic dark matter

(DM) profile predicted by the Ruffini–Argüelles–Rueda (RAR) model (Ruffini, Argüelles & Rueda 2015; Argüelles et al. 2018). In the RAR model, the DM distribution in galaxies is obtained from the general relativity field equations, assuming it as a self-gravitating system of fermions at finite temperature in equilibrium and distributed in phase space according to the Fermi–Dirac statistics including a particle energy cut-off that gives to the configuration, a finite size (see Argüelles et al. 2018, for more details). We hereafter refer to these neutral, massive DM fermions as '*darkinos*'. The RAR model leads to a *dense core–diluted halo* density profile in which the darkinos are: (1) in a quantum degenerate regime within the nearly uniform core, (2) followed by an intermediate quantum-classical regime in the density fall-off and plateau phase, and (3) finally in a Boltzmann regime in the outer halo that follows a power-law density ending with a nearly exponential cut-off defining the galaxy border. There is a bunch of astrophysical consequences of the *core–halo* profile of darkinos derived from the RAR model. In Argüelles et al. (2018), it has been shown that it explains the rotation curves of the Milky Way outer halo. In Argüelles et al. (2019), this agreement has been shown to apply as well to other galaxy types ranging from dwarfs to big ellipticals and galaxy clusters. These results have further enticed attention on the darkinos microphysics, e.g. their self-interactions (Argüelles et al. 2016; Yunis et al. 2020a) and interaction with neutrinos (Penacchioni, Civitarese & Argüelles 2020) as well as in their macrophysics, e.g. their lensing properties (Gómez et al. 2016), their influence in the dynamics of binaries (Gómez & Rueda 2017), their halo formation and stability on cosmological time-scales (Argüelles et al. 2020), and their role in the large- and small-scale structure formation (Yunis, Argüelles & López Nacir 2020b).

★ E-mail: eduar.becerra@icranet.org (EAB-V); jorge.rueda@icra.it (JAR); ruffini@icra.it (RR)

Table 1. Summary of the inferred best-fitting parameters of the BH model and the RAR model of darkinos using the astrometry data of the 17 best-resolved S-stars.

Star	Model	a (as)	e	r_p (as)	r_a (as)	i (°)	ω (°)	Ω (°)	P (yr)	t_p (yr)	$\bar{\chi}^2_X$	$\bar{\chi}^2_Y$	$\bar{\chi}^2_Z$	$\langle\bar{\chi}^2\rangle$
S1	RAR	0.5940	0.5530	0.2655	0.9225	119.48	122.22	342.34	165.93	2001.62	1.3368	1.6463	0.2661	1.0831
	BH	0.5937	0.5533	0.2652	0.9222	119.33	122.23	342.39	165.66	2001.63	1.5804	1.2103	0.2803	1.0237
S2	RAR	0.1252	0.8866	0.0142	0.2361	134.35	66.772	228.02	16.054	2018.38	1.5964	6.3411	1.5964	3.0725
	BH	0.1252	0.8863	0.0143	0.2362	134.35	66.450	227.97	16.051	2018.38	1.8004	7.2332	1.8004	3.3586
S4	RAR	0.3569	0.3895	0.2179	0.4958	80.942	290.82	258.82	77.508	2034.71	1.4043	2.0123	0.9533	1.4566
	BH	0.3568	0.3891	0.2180	0.4956	80.876	291.02	258.82	77.184	2034.58	1.6329	1.6882	0.9530	1.4247
S8	RAR	0.4036	0.8029	0.0796	0.7277	74.045	347.56	315.45	92.871	2076.51	4.7788	2.8926	0.9538	2.8751
	BH	0.4040	0.8028	0.0797	0.7283	74.358	346.86	315.46	92.989	2076.46	4.4261	2.5700	0.8988	2.6316
S9	RAR	0.2750	0.6430	0.0982	0.4518	82.682	150.58	156.71	52.259	2028.27	1.4582	1.1680	0.4809	1.0357
	BH	0.2745	0.6425	0.0981	0.4509	82.532	150.43	156.70	52.081	2028.31	1.2234	1.4709	0.4834	1.0592
S12	RAR	0.2986	0.8812	0.0334	0.5638	33.374	318.09	230.10	59.232	2054.98	1.1906	1.6396	0.1657	0.9986
	BH	0.2988	0.8883	0.0334	0.5642	33.520	317.98	230.37	59.145	2054.90	1.4464	1.5421	0.1640	1.0508
S13	RAR	0.2630	0.4275	0.1506	0.3754	24.479	245.15	74.887	48.856	2004.88	2.1403	0.7632	0.1324	1.0120
	BH	0.2631	0.4260	0.1510	0.3751	24.479	245.26	74.942	48.860	2004.90	2.2392	0.7807	0.1326	1.0508
S14	RAR	0.2890	0.9564	0.0126	0.5654	100.66	337.71	226.30	56.422	1999.72	2.0007	1.6106	1.1548	1.5887
	BH	0.2889	0.9564	0.0126	0.5652	100.40	336.74	226.46	56.232	1999.79	1.4896	1.9268	1.2899	1.5688
S17	RAR	0.3563	0.3973	0.2148	0.4979	96.624	324.19	191.63	77.315	2067.95	1.9937	1.3863	0.1222	1.1674
	BH	0.3568	0.3974	0.2150	0.4986	96.636	324.07	191.49	77.180	2067.78	1.9099	1.3733	0.1218	1.1350
S18	RAR	0.2383	0.4716	0.1259	0.3507	110.53	350.61	49.130	42.297	2036.18	1.0372	1.3511	1.0739	1.1541
	BH	0.2384	0.4715	0.1260	0.3508	110.53	349.87	49.174	42.154	2036.00	1.0055	2.6843	1.0648	1.5849
S19	RAR	0.5191	0.7510	0.1292	0.9088	71.910	155.20	344.66	135.46	2005.48	1.2719	2.4830	1.0759	1.6103
	BH	0.5190	0.7506	0.1295	0.9087	72.034	155.11	344.73	135.43	2005.40	1.8951	3.1838	0.8359	1.9716
S21	RAR	0.2192	0.7622	0.0521	0.3863	58.622	166.23	259.65	37.210	2027.64	1.2499	4.0652	0.2691	1.8614
	BH	0.2185	0.7629	0.0518	0.3852	58.630	165.64	259.67	36.984	2027.29	1.7393	3.7953	0.2540	1.9296
S24	RAR	0.9467	0.8908	0.1034	1.7900	103.53	289.93	7.9969	335.26	2024.69	1.6161	3.6132	0.1194	1.7829
	BH	0.9463	0.8907	0.1034	1.7892	103.53	289.93	7.9990	333.35	2024.77	1.2295	3.8249	0.1303	1.7282
S31	RAR	0.4472	0.5510	0.2008	0.6936	109.09	308.04	137.20	108.68	2017.98	2.2761	1.3093	1.5168	1.7007
	BH	0.4479	0.5508	0.2012	0.6946	108.93	307.93	137.19	108.56	2017.94	2.7348	1.2618	1.5448	1.8472
S38	RAR	0.1408	0.8175	0.0257	0.2559	170.98	18.053	99.694	19.182	2003.26	1.3141	2.6440	0.4762	1.4781
	BH	0.1411	0.8195	0.0255	0.2567	170.98	18.215	99.761	19.195	2003.31	1.3480	2.5486	0.4758	1.4575
S54	RAR	1.1985	0.8921	0.1293	2.2676	62.242	140.76	288.44	478.38	2004.30	1.1884	1.5459	0.2956	1.0099
	BH	1.1986	0.8927	0.1287	2.2685	62.188	140.79	288.44	475.18	2004.38	1.5915	1.1222	0.2922	1.0020
S55	RAR	0.1082	0.7206	0.0302	0.1861	149.93	331.33	325.45	12.905	2009.29	0.4437	2.0672	3.1088	1.8732
	BH	0.1083	0.7204	0.0303	0.1863	149.94	331.44	325.48	12.908	2009.30	0.4504	1.9576	3.1099	1.8393

Notes. a: semi-major axis of the orbit; e: eccentricity; r_p: distance to pericentre; r_a: distance to apocentre; i: inclination; ω: argument of pericentre; Ω: position angle of the ascending node; P: orbital period; t_p: epoch of pericentre passage; $\bar{\chi}^2_X$: reduced–χ^2 for X position; $\bar{\chi}^2_Y$: reduced–χ^2 for Y position; $\bar{\chi}^2_Z$: reduced–χ^2 for line-of-sight radial velocity; $\langle\bar{\chi}^2\rangle = \frac{1}{3}\left(\bar{\chi}^2_X + \bar{\chi}^2_Y + \bar{\chi}^2_Z\right)$.

Note: We refer to Becerra-Vergara et al. (2020) for details on the definition of the parameters and on the fitting procedure.
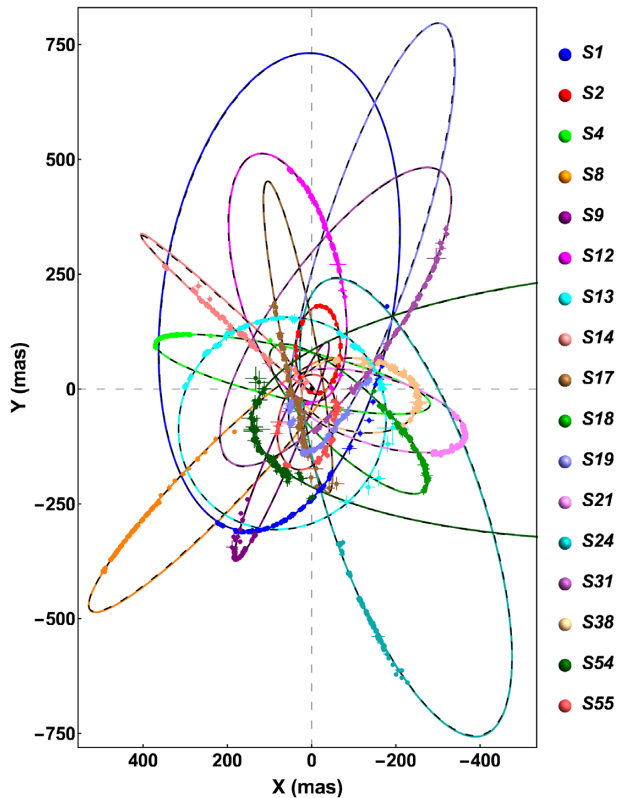
Figure 1. Best-fitting orbits for the 17 best-resolved S-star orbiting Sgr A∗. It shows the projected orbit on the sky, *X* versus *Y*, where *X* is right ascension and *Y* is declination. The *black dashed curves* correspond to the BH model and the *coloured curves* to the RAR model of darkinos. We refer to Table 1 for the orbital parameters of each star in both models. The astrometric measurements are taken from Gillessen et al. (2009a, 2017) and Do et al. (2019).

Having recalled the overall features of the darkinos of the RAR model, we turn now back to the topic of this letter. We have shown in Becerra-Vergara et al. (2020) that, for darkinos of 56 keV rest mass–energy, the spacetime geometry produced by the dense quantum core leads to geodesics which fit equally good, and definitely superior, respectively, the observational data of S2 and G2. This result has given a first observational support to the darkinos alternative nature of Sgr A∗. Our aim here is to go a step further and extend our previous analysis to the up-to-date astrometry data of the 17 best-resolved S-stars (Ghez et al. 2008; Gillessen et al. 2009b, 2017). In this way, we are testing the models with a more robust sample composed of a statistically significant number of stars with well-determined positions and velocities. This considerably improves our previous test with S2 complemented by the object G2 that is of a questioned nature (see e.g. Witzel et al. 2014; Ciurlo et al. 2020). We show below that the novel results here presented confirm and strengthen the alternative nature of Sgr A∗ as a dense core of darkinos.

2 GEODESICS AND ASTROMETRY DATA FIT

The monitoring of the S-stars around Sgr A∗ provides crucial knowledge about the properties of the gravitational potential of the massive object hosted by Sgr A∗. One of the most interesting S-stars is S2, whose orbit determination is less prone to errors being it the brightest. It describes a nearly elliptical orbit with one of the shortest orbital periods ($\approx$16 yr; see e.g. Ghez et al. 2003; Gillessen et al. 2017; Gravity Collaboration et al. 2018a), with its pericentre

being the second closest to Sgr A∗, $r_{p(S2)} \approx 0.6$ mpc. Therefore, S2 provides the most accurate constraints on the gravitational potential of Sgr A∗ to date (Ghez et al. 2008; Gillessen et al. 2009b, 2017).

We here follow the treatment described in appendices A and C of Becerra-Vergara et al. (2020) for the best-fitting procedure of S2 and G2, which has been used to constrain the model parameters in the two scenarios: the BH case and the (RAR) DM-core case. In the former, the relevant parameter associated with the source of the gravitational field is the BH mass (M_{BH}), and in the latter, the DM core mass (M_c). The value of M_c depends on the (underlying) free RAR parameters, including the darkino mass m (Argüelles et al. 2018), but the reduced-χ^2 minimization here applied to fit the orbits, following Becerra-Vergara et al. (2020), only uses M_c. For each M_c value applied in this procedure, the set of underlying free RAR model parameters is such that the overall *core–halo* RAR profile better fits the Galaxy rotation curve (see Appendix A of Becerra-Vergara et al. 2020 for further details). Then, we solve the full general relativistic equations of motion of a test particle in the set spacetime geometry and obtain the real geodesic which, projected on to the sky plane, best fit the apparent stellar orbit. At any given time, this is given by the measurements of the right ascension (*X*) and declination (*Y*). For a fixed model, the real orbit is determined once values of the energy and angular momentum per unit mass of the geodesic are given. They can be determined using the effective potential technique as described in Becerra-Vergara et al. (2020), by setting values for the pericentre and apocentre radii, r_p and r_a. Alternatively, r_p and r_a could be replaced by the semimajor axis *a* and eccentricity *e* of an effective ellipse. The values of r_p and r_a are not affected in the projection of the orbit on to the sky plane, so the apparent orbit is then determined for given values of the osculating orbital elements, i.e. ω, *i*, and Ω, respectively, the argument of pericentre, the inclination between the real orbit and the sky plane, and the ascending node angle. With this, the orbital period *P* and the time of closest approach to the GC, i.e. the time to reach the pericentre, t_p (in J2000 time convention; see Becerra-Vergara et al. 2020 for details), can be also inferred. Constant position offsets X_0 and Y_0 are also introduced to account for the relative position of the gravitational centre of mass to the reference frame (see equation C12 in Becerra-Vergara et al. 2020, and references therein). The procedure is performed in an iterative fashion to obtain the best-fitting parameters from least-squares minimization. In Becerra-Vergara et al. (2020), the application of this procedure to the case of S2 led to $M_{BH} = 4.075 \times 10^6$ M$_\odot$, in the BH model, and $M_c = 3.5 \times 10^6$ M$_\odot$, in the RAR model. This M_c value together with the overall rotation curve fit, implied the minimum allowed darkino mass, $mc^2 = 56$ keV, fulfilling all observational constraints. For this mass, the DM core radius is $r_c \approx 0.4$ mpc (Becerra-Vergara et al. 2020). Larger darkino masses (up to 345 keV), for the same M_c, imply more compact DM core sizes down to a few Schwarzschild radii, still satisfying the rotation curve data (Argüelles et al. 2018).

We emphasize the reliability of our fitting procedure. Our inferred value of M_{BH} in the BH case, using the S2 data, agrees with the most recently reported values, e.g. $M_{BH} = 4.1 \times 10^6$ M$_\odot$ by Gravity Collaboration et al. (2018a), and 3.975×10^6 M$_\odot$ by Do et al. (2019). We here extend the application of our model, previously tested with S2 and G2, to the other S-stars. We apply the above procedure keeping fixed the above parameters since they define the source of the gravitational field. Likewise, we fix $X_0^{BH} = -0.0830$ and $Y_0^{BH} = 2.4893$ (units of milliarcsecond), $X_0^{RAR} = -0.1557$, $Y_0^{RAR} = 2.5527$, and the distance to Sgr A∗, 8 kpc. We then search for the parameters that determine the real orbit and best fit the apparent one. We analyse the 17 best-resolved S-stars S1, S2, S4, S8, S9, S12, S13, S14, S17, S18, S19, S21, S24, S31, S38, S54, and S55 (Gillessen et al. 2017).
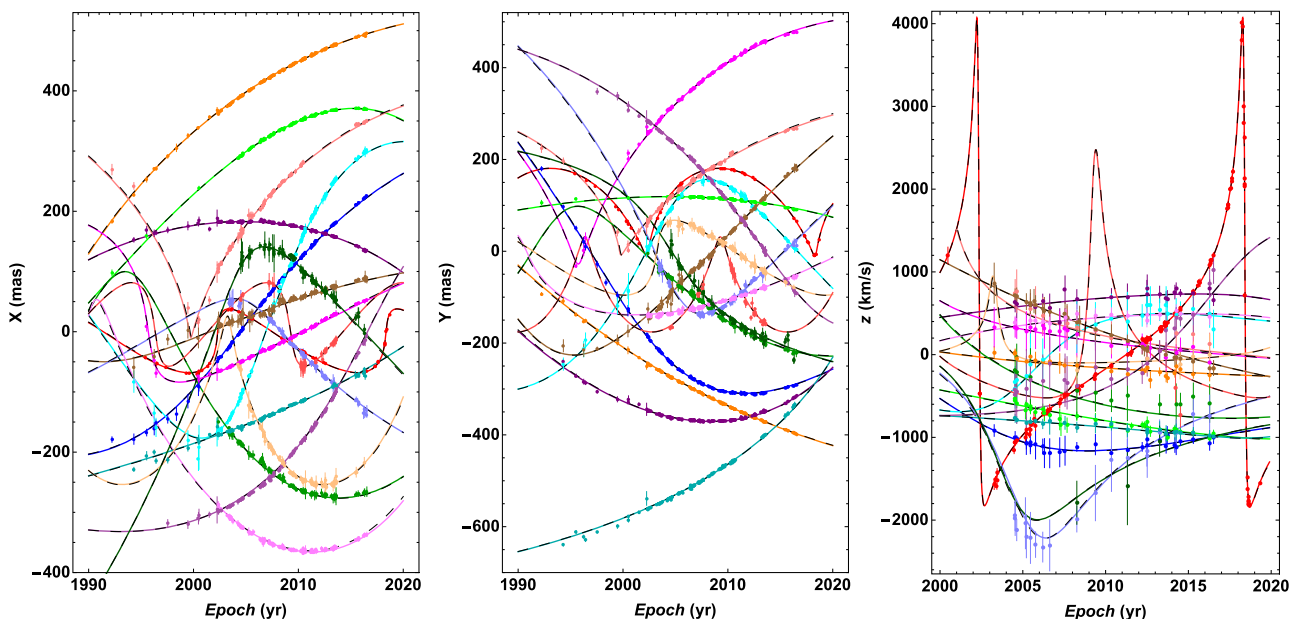
Figure 2. Best fit of the observed right ascension X (left-hand panel), declination Y (central panel), and line-of-sight radial velocity (redshift function) z (right-hand panel), as a function of time, for the 17 best-resolved S-star orbiting Sgr A∗. The *black dashed curves* correspond to the BH model and the *coloured curves* to the RAR model of darkinos. We refer to Table 1 for the orbital parameters of each star in both models. The astrometric measurements are taken from Gillessen et al. (2009a, 2017) and Do et al. (2019).

3 DISCUSSION AND CONCLUSIONS

Table 1 summarizes the best-fitting model parameters and the corresponding reduced-χ^2 for the position (X and Y) and the line-of-sight radial velocity (i.e. the redshift function z), for the central BH and the RAR DM models. We can see that, overall, the RAR model performs slightly better than the BH model. An estimate of the performance can be obtained by calculating the average of the averages, namely to sum up the values of the last column of Table 1, and divide it by the sample number. For the RAR model, this estimate leads to 1.5741, and for the BH model, 1.6273. This confirms their comparable accuracy in describing the S-stars data, being the RAR model of darkinos slightly preferred.

We can gain information on the reliability of our fitting procedure by comparing the inferred parameters in the BH case. We have recalled in Section 2 that our BH mass inference using S2 data agrees with most of the recent values reported in the literature using the same object. In addition, it also agrees with the reported value obtained from the simultaneous fit of several stellar orbits: Boehle et al. (2016) reported $M_{BH} = (4.02 \pm 0.16) \times 10^6 \, M_\odot$ using S2 and S38, and Parsa et al. (2017) reported $M_{BH} = (4.15 \pm 0.13) \times 10^6 \, M_\odot$ using S2, S38, and S55. This is further confirmed by the fact that our inferred orbital parameters for the BH model (see Table 1) do not differ by more than 2 per cent for S2, 1 per cent for S38, and 3 per cent for S55 from the values reported in Parsa et al. (2017). Our inferred value of M_{BH} is also within the window reported in Gillessen et al. (2017), $M_{BH} = (4.28 \pm 0.21) \times 10^6 \, M_\odot$, for the 17 S-stars. While these estimates of M_{BH} in the existing literature used post-Newtonian approximations, our method is fully general relativistic (see Becerra-Vergara et al. 2020).

Having said this, we can turn to the visualization of the orbits. Fig. 1 shows the data and a comprehensive plot of the best fit of the observed orbits of the sample of 17 S-stars, including the stars with the most compact orbits (S2, S38, and S55). The similar performance of the RAR and BH models is evident, being their differences almost

indistinguishable at these scales. In Fig. 2, we present the data and the best fit of the time evolution of the star position components, $X(t)$ and $Y(t)$, as well as the redshift function, $z(t)$, for the S-star sample. Also in this case, the similar performance of the two tested models is evident. This is particularly relevant because that a model provides an accurate fit of the orbit, i.e. of X versus Y, does not necessarily imply that it correctly fits its time evolution, namely the model must correctly predict the observed star motion. Therefore, as described in Becerra-Vergara et al. (2020), the estimation of the goodness of the fit must compare the theoretical values of X, Y, and z with the measured values at each observational time.

Summarizing, this letter shows for the first time that a highly dense concentration of DM particles sited at the GC can explain the dynamics of the S-stars with similar (and some cases better) accuracy compared to a central BH model. These results strengthen the alternative nature of Sgr A∗ as a dense quantum core of darkinos superseding the central massive BH scenario. There is the key additional fact that this very same *core–halo* distribution of 56 keV darkinos also explains the rotation curves of the Milky Way (see Argüelles et al. 2018; Becerra-Vergara et al. 2020, for details). For particle masses ~ 100 keV, the core radius shrinks from 0.4 mpc to a few Schwarzschild radii, so the gravitational potential produced by a central BH of mass M_{BH} and a (RAR) DM core of mass $M_c = M_{BH}$, practically coincide for $r \gtrsim 10 \, GM_{BH}/c^2$ (Gómez et al. 2016). Therefore, the dynamics of baryonic matter at these scales should not differ much in the two scenarios. This becomes relevant for the dynamics of objects in the vicinity of Sgr A∗, e.g. the recently detected *hot-spots* claimed to move in a circular orbit of 7–23 GM_{BH}/c^2 radius (Gravity Collaboration 2018b; Matsumoto, Chan & Piran 2020). However, this wide range of values shows how the inferred real orbit is strongly affected by model assumptions and the relatively poor quality of the spots astrometry data, which is not comparable with the S-stars data here used. The dynamics of these spots remain an interesting target for future investigation as the quantity and quality of the data improve. In this line, the recent

observations of a new set of S-stars (S62, S4711–S4714), possibly reaching pericentre distances $\sim 400\ GM_{BH}/c^2$ (Peißker, Eckart & Parsa 2020a; Peißker et al. 2020b), could also offer the possibility to further constrain the DM core size around Sgr A∗, likewise the lower limit of the darkino mass.

We would like to outline some additional astrophysical and cosmological consequences of the *core–halo* distribution of darkinos in the RAR model. First, it has been shown in Argüelles et al. (2019) that the DM RAR profiles are *Universal*, thereby can be also successfully applied to dwarfs, ellipticals, and galaxy clusters, for $m \approx 50\,\mathrm{keV}$. Secondly, a crucial question that arises is whether or not a DM profile with this morphology can be formed in a cosmological framework. Importantly, it has been recently demonstrated in Argüelles et al. (2020) that such *core–halo* profiles are natural outcomes within non-linear structure formation in warm DM cosmologies, when the fermionic (quantum) nature of the DM particles is accounted for. It has been there shown that these novel DM profiles either are thermodynamically and dynamically stable for the lifetime of the Universe, or eventually collapse into a supermassive BH if a critical (threshold) mass of the quantum core is reached. This provides a new appealing scenario for the formation, starting from a DM seed, of the supermassive BHs observed in active galactic nuclei (AGNs), with key implications for AGN astrophysics and early cosmology (Argüelles et al. 2020).

ACKNOWLEDGEMENTS

DATA AVAILABILITY

The astrometric data used in this work were obtained from Gillessen et al. (2009a, 2017) and Do et al. (2019), and the data here generated are available in Table 1.

REFERENCES

Argüelles C. R., Mavromatos N. E., Rueda J. A., Ruffini R., 2016, J. Cosmol. Astropart. Phys., 4, 038

Argüelles C. R., Krut A., Rueda J. A., Ruffini R., 2018, Phys. Dark Universe, 21, 82

Argüelles C. R., Krut A., Rueda J. A., Ruffini R., 2019, Phys. Dark Universe, 24, 100278

Argüelles C. R., Díaz M. I., Krut A., Yunis R., 2020, MNRAS, 502, 4227

Becerra-Vergara E. A., Argüelles C. R., Krut A., Rueda J. A., Ruffini R., 2020, A&A, 641, A34

Boehle A. et al., 2016, ApJ, 830, 17

Bouffard É., Haggard D., Nowak M. A., Neilsen J., Markoff S., Baganoff F. K., 2019, ApJ, 884, 148

Ciurlo A. et al., 2020, Nature, 577, 337

Do T. et al., 2019, Science, 365, 664

Genzel R., Eisenhauer F., Gillessen S., 2010, Rev. Mod. Phys., 82, 3121

Ghez A. M. et al., 2003, ApJ, 586, L127

Ghez A. M., Salim S., Hornstein S. D., Tanner A., Lu J. R., Morris M., Becklin E. E., Duchêne G., 2005, ApJ, 620, 744

Ghez A. M. et al., 2008, ApJ, 689, 1044

Gillessen S., Eisenhauer F., Trippe S., Alexander T., Genzel R., Martins F., Ott T., 2009a, ApJ, 692, 1075

Gillessen S., Eisenhauer F., Fritz T. K., Bartko H., Dodds-Eden K., Pfuhl O., Ott T., Genzel R., 2009b, ApJ, 707, L114

Gillessen S. et al., 2017, ApJ, 837, 30

Gillessen S. et al., 2019, ApJ, 871, 126

Gómez L. G., Rueda J. A., 2017, Phys. Rev. D., 96, 063001

Gómez L. G., Argüelles C. R., Perlick V., Rueda J. A., Ruffini R., 2016, Phys. Rev. D., 94, 123004

Gravity Collaboration, 2018a, A&A, 615, L15

Gravity Collaboration, 2018b, A&A, 618, L10

Gravity Collaboration, 2020, A&A, 636, L5

Matsumoto T., Chan C.-H., Piran T., 2020, MNRAS, 497, 2385

Parsa M., Eckart A., Shahzamanian B., Karas V., Zajaček M., Zensus J. A., Straubmeier C., 2017, ApJ, 845, 22

Peißker F., Eckart A., Parsa M., 2020a, ApJ, 889, 61

Peißker F., Eckart A., Zajaček M., Ali B., Parsa M., 2020b, ApJ, 899, 50

Penacchioni A. V., Civitarese O., Argüelles C. R., 2020, Eur. Phys. J., 80, 183

Plewa P. M. et al., 2017, ApJ, 840, 50

Ruffini R., Argüelles C. R., Rueda J. A., 2015, MNRAS, 451, 622

Witzel G. et al., 2014, ApJ, 796, L8

Yuan F., Narayan R., 2014, ARA&A, 52, 529

Yunis R., Argüelles C. R., Mavromatos N. E., Moliné A., Krut A., Carinci M., Rueda J. A., Ruffini R., 2020a, Physics of the Dark Universe, 30, 100699

Yunis R., Argüelles C. R., López Nacir D., 2020b, J. Cosmol. Astropart. Phys., 2020, 041

This paper has been typeset from a TEX/LATEX file prepared by the author.